Journal of Tissue Engineering
4: 2041731413508771

DOI: 10.1177/2041731413508771
tej.sagepub.com
SAGE

Porcine incisional hernia model: Evaluation of biologically derived intact extracellular matrix repairs

Gary A Monteiro[1], Aubrey I Delossantos[1], Neil L Rodriguez[1], Paarun Patel[1], Michael G Franz[1] and Christopher T Wagner[1,2]

Abstract

We compared fascial wounds repaired with non-cross-linked intact porcine-derived acellular dermal matrix versus primary closure in a large-animal hernia model. Incisional hernias were created in Yucatan pigs and repaired after 3 weeks via open technique with suture-only primary closure or intraperitoneally placed porcine-derived acellular dermal matrix. Progressive changes in mechanical and biological properties of porcine-derived acellular dermal matrix and repair sites were assessed. Porcine-derived acellular dermal matrix–repaired hernias of additional animals were evaluated 2 and 4 weeks post incision to assess porcine-derived acellular dermal matrix regenerative potential and biomechanical changes. Hernias repaired with primary closure showed substantially more scarring and bone hyperplasia along the incision line. Mechanical remodeling of porcine-derived acellular dermal matrix was noted over time. Porcine-derived acellular dermal matrix elastic modulus and ultimate tensile stress were similar to fascia at 6 weeks. The biology of porcine-derived acellular dermal matrix–reinforced animals was more similar to native abdominal wall versus that with primary closure. In this study, porcine-derived acellular dermal matrix–reinforced repairs provided more complete wound healing response compared with primary closure.

Keywords

Incisional hernia, biologic mesh, biologic tissue matrix, Strattice, fascial wounds

Received: 30 July 2013; accepted: 23 September 2013

Introduction

Ventral incisional hernias are a complication of abdominal wall surgery. The general objective for successful closure of these hernias is to create a repair capable of withstanding the everyday mechanical loads of the abdominal wall. Procedures for the repair of incisional hernias with sutures alone or reinforced with surgical mesh have been reported. However, the effectiveness of the two repair modes is not fully understood. Luijendijk et al.,[1] in a prospective randomized study, reported that a retrofascial preperitoneal repair with polypropylene mesh is superior to suture-only repair with regard to hernia recurrence. However, the biology and the mechanism of repair of the two modes of fascial closure have not been completely evaluated.[1–3] Even less information is available to determine the efficacy of hernia wounds repaired with biologically derived intact extracellular matrix (ECM) materials.

Biologically derived intact ECM materials are collagen grafts harvested from human or animal dermis, pericardium, or intestinal membranes. In general, they are processed to remove cells and xenogeneic response epitopes and are believed to more readily integrate with native tissue and be more biocompatible compared with synthetic mesh.[4–6] Additionally, such materials have found a niche in contaminated fields as they are believed less likely to exacerbate an infection compared with synthetic materials.[7,8] As a result, they are becoming increasingly popular for use in incisional hernia repairs. Implanted biologically derived intact ECM materials used for hernia repair begin to remodel once implanted in vivo.[9–11] The biological response of resident abdominal wall inflammatory cells and the

[1]LifeCell Corporation, Inc., Branchburg, NJ, USA
[2]Department of Biomedical Engineering, The College of New Jersey, Ewing, NJ, USA

Corresponding author:
Gary A Monteiro, LifeCell Corporation, Inc., One Millennium Way, Branchburg, NJ 08876, USA.
Email: gmonteir@gmail.com

collagen synthesis of abdominal wall fibroblastic cells within a biological matrix used for hernia repair will modulate the integrity and mechanical properties of the repair over time. Previous work has demonstrated that the cell response is dependent on the wound pathology. DuBay et al.[12–14] reported a significant decrease in collagen synthesis and, ultimately, the wound bed material properties of herniated abdominal wall defects compared with an acute myofascial defect model.

Current animal models used to evaluate the effectiveness of hernia repairs are lacking in either biological or mechanical function requirements. The surgical community worldwide recognizes the need for additional animal models to further develop prosthetic materials and techniques for hernia repair.[15,16] Acute hernia models do not capture the biology of chronic hernia wounds, which result in an increased hernia recurrence rate.[14] Small-animal hernia models, such as the one used by DuBay et al.,[12–14] provide an opportunity to understand the biology of hernia repair; however, they fall short in addressing the loading characteristics of the human abdominal wall. Furthermore, young and healthy rats used for research purposes may obscure the true effectiveness of any repair due to their robust innate repair mechanisms. The porcine model developed by Melman et al.[17] approaches a true incisional hernia model. It allows an incision defect to herniate and mature over time prior to repair. The loading characteristics of a porcine model provide a realistic comparison to the human abdominal space.[17] The limitation in this model lies in the location and the size of defects created, utilizing a bilateral incisional defect on either side of the midline over the external oblique muscles. Healing in muscle tissue is aided by the substantial vasculature present to sustain function. It is more common for clinicians to incise the less-vascularized linea alba to access the abdominal cavity during surgeries. The limited vasculature present in the linea alba makes it a more challenging repair site because it is prone to herniation if weakened.

The purpose of this study was to develop a large-animal incisional hernia model that is clinically relevant and to evaluate the efficacy of biologically derived matrix material. We developed a porcine incisional hernia model that simulates the large and challenging hernias surgeons face on a daily basis. The model recreates both the biological response as well as the mechanical challenges that accompany complex and challenging hernias. We utilized this model to compare the efficacy of hernia repairs with suture-alone closure and biologic matrix–reinforced closure. We have also assessed the remodeling of biological matrices processed by using Strattice™ Reconstructive Tissue Matrix (LifeCell Corporation, Branchburg, NJ, USA) implanted in the abdominal space over time to better define the role of biologically derived matrices for incisional hernia repair.

Methods

Mesh preparation

Non-cross-linked intact porcine-derived acellular dermal matrix (PADM) was prepared as per Connor et al.[9] Materials prepared were terminally sterilized and presented biological and mechanical characteristics as previously described.[9] Briefly, porcine dermal tissue was obtained from 6-month-old farm-raised pigs. Following euthanasia, pigs were subjected to a brief hot-water treatment. The porcine hides were then removed from the animals, mechanically leveled, and removed of hair. Leveled and split hides (thickness of 1.3 ± 0.5 mm) were then processed by using proprietary Strattice-processing methods. Intentional hide-to-hide variation was included in the study to avoid hide bias and was tracked by PADM number. Hide-to-hide variation was accounted for in future analyses by normalizing all values to day 0 measurements for that particular PADM number.

Animal model

Skeletally mature Yucatan pigs (LoneStar Laboratory Swine, Sioux Center, IA, USA) weighing 55–85 kg were acclimated and housed under standard conditions. Animals were allowed ad libitum intake of standard chow and water throughout the study. All animal care and operative procedures were performed in accordance with the US Public Health Service Guide for the Care of Laboratory Animals (National Institutes of Health (NIH) Publication No. 86-23, revised 1985) and were approved by the study site Institutional Animal Care and Use Committee. Animals were randomized to the control group of suture-only repair ($n = 5$) or the experimental group of PADM repair ($n = 16$). All animals were fasted 16 h prior to surgery. After anesthetizing the animals with telazol 4.4 mg/kg and isoflurane gas 2 mg/kg, animals were prepped for surgery. Preparations included shaving the underbelly and prepping the surgical site with 70% alcohol and betadine. A tolazoline 4 mg/kg injection was used as a xylazine-reversing agent following preparations. Ceftiofur 5 mg/kg was used to prevent bacterial infections. Ketoprofen 2 mg/kg, fentanyl patch 50 µg/h, and buprenorphine were administered for pain relief.

Incisional hernia creation

A 6.5-cm wide × 13-cm long, semicircular, full-thickness skin flap 1.5 cm lateral to the midline was raised through the avascular prefascial plane. The 1:2 ratio of flap length to width was maintained to prevent flap ischemia. A 10-cm full-thickness laparotomy incision was made through the fascia of the midline linea alba. The peritoneum sac immediately below the fascial incision was cut, taking care not to puncture or pinch the bowels during the procedure. A biopsy for gene expression analysis was collected at the

Figure 1. Ultrasound image of herniated abdominal wall at 3 weeks post incision. A Toshiba Viamo ultrasound machine with a 5-MHz catheter probe was used to image hernias prior to hernia repair. Arrow indicates location of incision defect. The left abdominal rectus is present in image and is identified as the dense oblong structure to the left of the defect.

incision site. Care was taken to excise biopsies away from the cauterized fascia. The fascial incision was closed with five interrupted, absorbable 2-0 BIOSYN™ sutures (Covidien, Mansfield, MA, USA) placed 0.5 cm from either end of the laparotomy incision and 1.5 cm apart. The skin flap was then replaced and a two-level closure was used to prevent intestinal evisceration. A 2-0 BIOSYN subcuticular running stitch was used as a first level of support, and a 3-0 BIOSYN suture was used to close the cuticular layer. Cyanoacrylate was used as a topical over the skin incision to avoid infections.

Immediately following the creation of the incision, the animal's abdominal space was imaged using a Toshiba Viamo™ ultrasound machine (Toshiba Medical Systems, Tustin, CA, USA). After 30–60 min of recovery under heat lamps, the pigs were returned to fresh individual pens.

All animals had visible large bulging ventral defects contained by the skin flap within 1 week of repair. The defects were allowed to mature for 3 weeks before repair. At 3 weeks, defects were repaired with either suture-only closure or with PADM closure. Standard ultrasound images were recorded to visualize hernia formation prior to repair (Figure 1).

Hernia repair

Skin flaps were reraised following the original incisional hernia skin flap scars. Blunt dissection was used to release the flap over the fascial plane and expose the ventral defect. The size and shape of the defect formed were measured using a graduated ruler. The adhesion of the omentum and any other abdominal cavity contents to the skin flap were bluntly dissected away and returned to the abdominal cavity. If blunt dissection was insufficient to release adhesions from the flap, a cutting knife was used to release the adhesions. Precautions were taken to avoid puncturing the intestines during hernia repair. For the purpose of consistency, the hernia sites of all animals were extended to 10 cm in length prior to closure. A biopsy for gene expression analysis was collected at the hernia ring. The suture-only group was closed using a 0 PROLENE™ (Ethicon, Somerville, NJ, USA) suture in a continuous fashion across the abdominal rectus muscles. The PADM group received a 12 × 8-cm (approximately) matrix placed intraperitoneally and sutured in an oval pattern around the defect using a 0 PROLENE suture. The PADM was not buttressed to the abdominal rectus but instead fastened tight against the abdominal wall using a parachuting technique, which allowed maximum contact between the abdominal wall and matrix material within the oval patterned outline. A resorbable 0-0 BIOSYN suture was used to close the midline over the PADM. The skin flap for both the PADM and suture-only groups was closed at two levels, as was done during the incision creation. Following repair of the defects, the site was imaged using ultrasound to confirm containment of abdominal content.

Explants

At scheduled explant times (2, 4, and 6 weeks), animals were euthanized, skin flaps were raised, and the PADM was excised en bloc with surrounding abdominal wall muscles and tissue (Figure 2). Biopsies of tissue within and away from the PADM were taken and flash frozen in liquid nitrogen for gene expression evaluation. PADM size measurements were approximated and general observations were noted. Explants were shipped under Roswell Park Memorial Institute medium on wet ice for mechanical evaluation. On receipt of explants at the mechanical test facility, gross observations were rerecorded. The extent of PADM adhesion to the peritoneum was recorded. Any damage or disruptions in the tissue or wound site were also noted. PADM anchoring sutures were cut and the PADM was blunt dissected away from the peritoneum. Samples for mechanical testing were harvested from the freed PADM. Histopathology samples were harvested from three regions on the PADM: at the suture interface, within the herniation site, and outside the herniation site. Locations of mechanical samples on the PADM and relative to the abdominal wall incision were recorded. All mechanical samples were approximately 1 × 6 cm. Histology samples were approximately 1 × 1 cm.

Mechanical testing of PADM

Pre-implanted materials were cut into 1 × 6-cm strips for mechanical evaluation. Implanted PADM was blunt dissected away from the peritoneum and cut into 1 × 6-cm strips for mechanical evaluation. Orientation (sagittal or transverse) and location of each piece (with reference to hernia ring and suture locations) were recorded. Permanent

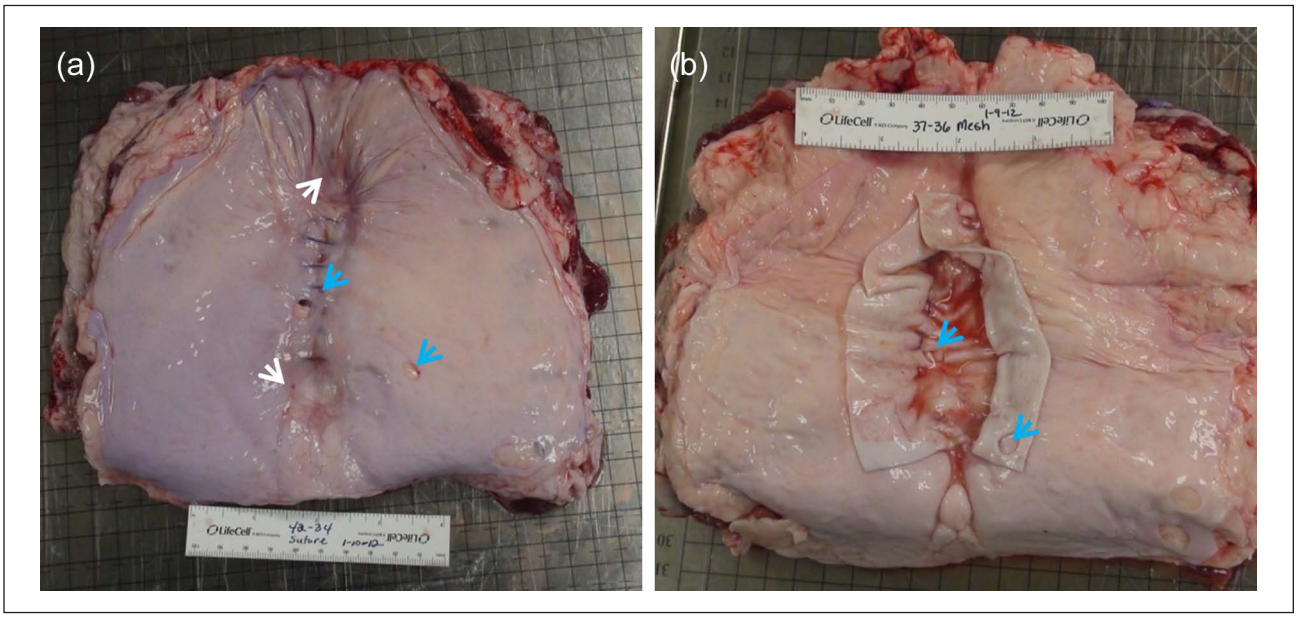

Figure 2. Representative image of suture-only and non-cross-linked intact porcine-derived acellular dermal matrix (PADM) explants. (a) Scarring along the suture line in the muscle layer and dimpling in the abdominal wall, above and below the suture line (white arrows) in the suture-only repair group. (b) Minimum scarring was noted in the PADM-reinforced animals. Biopsy punches are designated by blue arrows.

sutures were removed from the PADM, and the samples were washed in phosphate-buffered saline for at least 2 h prior to testing. Each mechanical evaluation strip was clamped at each end within the pneumatic grips of an Instron 5865 tensile tester (Instron Corporation, Norwood, MA, USA) equipped with a 1000-N load cell. Prior to tensile testing, surrounding connective tissue was excised and sample thicknesses were measured using a Mitutoyo Low Force Digital Indicator (Mitutoyo America Corporation, Aurora, IL, USA). A gauge length of 4 cm was used, and a preload of 0.5 N (tension) was applied prior to testing. Samples were tensile tested at a strain rate of 1.65%/min until a 40% decrease in load occurred, at which point testing was terminated and the maximum load (measured in newtons (N)) was determined as the failure strength of the PADM. Following testing, stress, strain, and Young's modulus were calculated using standard algorithms in Bluehill 2 software (Instron Corporation).

Mechanical testing of explanted muscle

To determine host primary healing strength, 1 × 8-cm longitudinal muscle sections were explanted from the abdominal wall superior to the implant across the suture line along the linea alba from each animal. For suture-only repairs, muscle sections across the suture line of the primary repair were harvested. Permanent sutures were removed from the suture-only closures prior to tensile testing. Host porcine tissue was clamped at each end within cryomechanical grips (Bose Corporation, Eden Prairie, MN, USA) on an Instron 5865 tensile tester equipped with a 1000-N load cell. Samples were clamped so as to place the incision line of the tissue between the two grips. A preload of 0.5 N (tension) was applied prior to testing, and a gauge length of 4 cm was used. Samples were tensile tested at an extension rate of 1.65%/min until a 40% decrease in load occurred, at which point testing was terminated and the maximum load was determined as the healing strength.

Histology

Explant samples inclusive of the graft midportion, graft–host tissue interface, and adjacent porcine host tissue were placed in 10% formalin for fixation and subsequent histologic analysis. Formalin-fixed samples were embedded in paraffin, sectioned (5 mm), and attached to glass slides. Sections were stained with hematoxylin and eosin (H&E). A subject matter expert reviewed and scored the slides for recellularization, revascularization, and inflammation.

Recellularization was analyzed by the demonstrated presence of cells (fibroblasts) within the portion of the test article section that was identified as PADM based on the reticular structure using H&E-stained slides. Cell repopulation was scored from 0 to 3, with a score of 0 representing "no cells present in the implanted intact ECM scaffold" and a score of 3 representing "significant fibroblastic cell presence in the ECM scaffold." Likewise, revascularization and inflammatory cell penetration were also assessed on a scale of 0–3, with 0 representing "none" and 3 representing "significant."

Microarray analysis

At least three samples in each group were analyzed using microarray analysis. Porcine genome-wide expression was examined for a total of 43,803 genes with Agilent Porcine GE 4 × 44K (Agilent Technologies, Santa Clara, CA, USA) by Genus Biosystems (Northbrook, IL, USA). Briefly, RNA was extracted and purified using Ambion® RiboPure™ (Ambion, Austin, TX, USA) RNA isolation. Total RNA samples were quantitated by ultraviolet spectrophotometry (OD260/280). Quality of total RNA was assessed using an Agilent Bioanalyzer. First- and second-strand complementary DNA (cDNA) was prepared from the total RNA samples. Complementary RNA (cRNA) target was prepared from the DNA template and verified on the Bioanalyzer. cRNA was fragmented to uniform size and hybridized to Agilent Porcine GE 4 × 44K arrays. Slides were washed and scanned on an Agilent G2565 Microarray Scanner. Data were analyzed with Agilent Feature Extraction and GeneSpring GX v7.3.1 software packages (Agilent Technologies). A heat map (with red representing genes that were highly upregulated, blue representing genes that were highly downregulated, and in-between levels of expression ranging from orange to green) was constructed by hierarchical clustering on highly differentially expressed genes, as defined by at least a twofold (t-test p value of < 0.05) difference between the suture-only versus PADM groups at 6 weeks.

Statistical analysis

All statistical analyses were performed in Minitab version 16. Normality was evaluated using the Anderson–Darling test for normality. Data that were normally distributed were evaluated using a one-way analysis of variance (ANOVA) followed by Tukey's post hoc test to determine significance across groups. Data that were not normally distributed were evaluated using nonparametric statistics. The Kruskal–Wallis test was used to determine difference across non-normal distribution groups followed by a Mann–Whitney post hoc test to determine significance across groups. For all statistical evaluations, the significance level was set to 0.05.

Results

Hernia formation

Of 21 incised animals, 15 (71%) formed an incisional hernia, defined as a visible protrusion of the abdominal contents or a hernia sac through the created incision. Ultrasound was used to visualize hernias (Figure 1). Despite visible bulging, not all animals had an overt hernia. Such animals were incised (10-cm defect) at the time of repair and closed as per group designation. The herniated animals were redistributed from their prospective group assignments to include at least three animals in each repair subgroup. On average, an elliptical-shaped hernia ring of dense scar tissue was observed. The median size of the hernia ring was 6 cm (long axis) × 2 cm (short axis). The hernia ring and skin flap immediately above the incision defect presented a sheen consistent with a mesothelial cell layer formation.

The most commonly observed defect included 50%–60% of the visible omentum protruding through the hernia ring with the formation of incomplete hernia sacs. Adhesions of the omentum to the skin flap were easily detached using blunt dissection techniques.

Gross observations at time of explants

No reherniations were observed in any animal following repair. One suture-only repair had a suture failure; however, no bowel tissue was noted protruding through the incision repair line. Dimpling was noted in the abdominal walls of suture-only repaired animals above and below the suture line at 6 weeks (Figure 2(a)). All suture-only repaired animals showed pronounced scarring along the suture line in the fascia behind the peritoneum. Scarring in PADM-reinforced animals was observed localized at the suture knot locations and was substantially less than scarring present in suture-only controls. Omentum attachment to the PADM was the most common adhesion. All omentum attachment was easily dissected and detached using blunt dissection techniques. Two PADM-reinforced animals had liver adhesions to a suture line at 2 and 4 weeks, which were easily dissected away with blunt dissection. One PADM-reinforced animal had substantial liver attachment to a suture corner at 6 weeks.

In PADM-reinforced animals, increased attachment of the PADM to the peritoneum was noted over time. At 6 weeks, the PADM between the suture windows was attached to the peritoneum. Some PADM overlap regions, beyond suture window, were also attached (Figure 2(b)). Visible vasculature ingrowth was noted in all PADM at 4 and 6 weeks, when attached to peritoneum.

Histology

Rapid cell infiltration and vasculature formation were noted in all PADM-reinforced animals (Figure 3). No differences were noted between herniated and nonherniated animals. Inflammation in the PADM group was mild and limited to suture locations. Inflammation in the suture-only group was comparable to the PADM group at week 6. Inflammation in fascia surrounding the PADM was minimal for both suture-only and PADM groups (Figure 4, Table 1).

Pronounced red staining was noted in histology of suture-only group samples. Palpitation of the site at the time of gross observations presented as hard nodules. This was assumed to be calcification. Calcification was present in the fascia/peritoneum complex juxtaposed to the suture

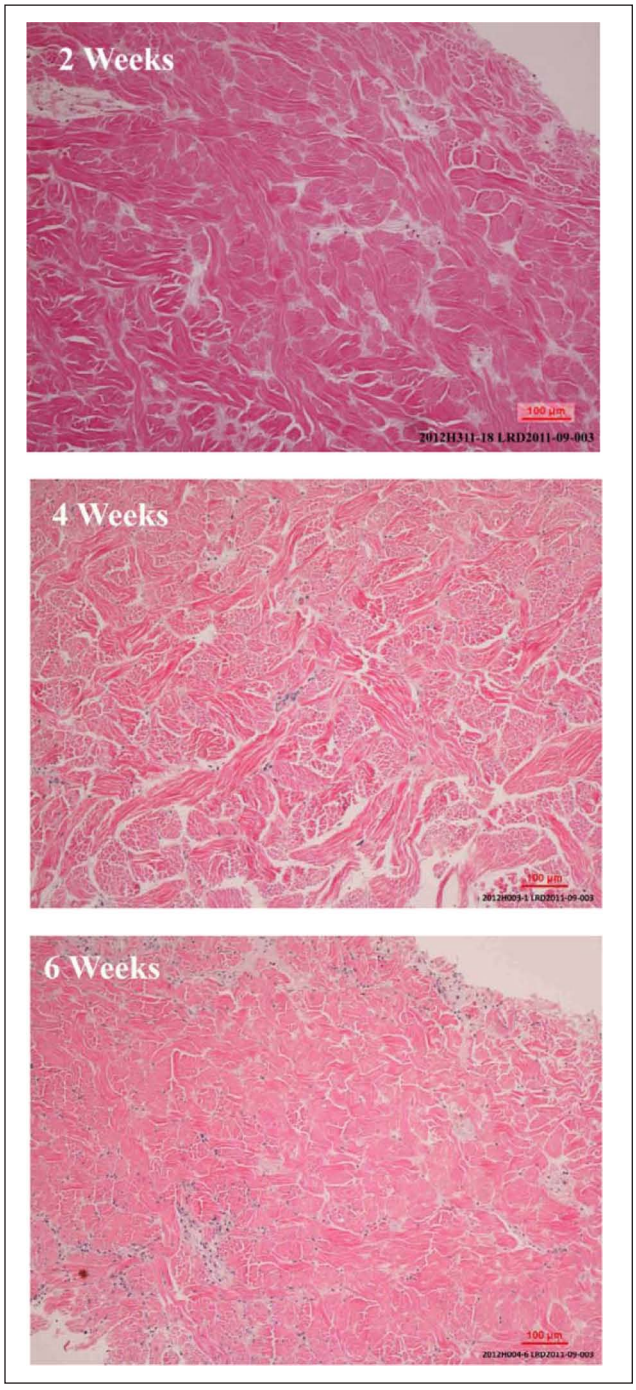

Figure 3. Hematoxylin and eosin staining of grafted non-cross-linked intact porcine-derived acellular dermal matrix over time. Cell infiltration (blue nuclei) and revascularization (bright eosinophilia) are notably increased over time.

closure. No calcification was noted in the PADM or in the fascia peritoneum complex of the PADM group at 2 and 4 weeks. At 6 weeks, one animal in the PADM group had a small region (<0.1 mm) of pronounced red H&E staining in the fascia peritoneum complex, presumed to be associated with suture (Figure 4).

Mechanical remodeling of PADM

Retrospective comparisons of the ultimate tensile strength and Young's modulus of nonherniated and herniated animals were conducted to determine whether failure to herniate adversely affected healing in this subpopulation. A general linear model with hernia formation, PADM number, and direction of testing as model factors was used to demonstrate significant differences between these groups. Both hernia formation and PADM number were deemed significant (ultimate tensile strength, ANOVA: $p < 0.0001$ and $p < 0.0001$, respectively; Young's modulus, ANOVA: $p < 0.0001$ and $p < 0.0001$, respectively). As such, the six nonherniated animals represent a distinct population of the cohort and were excluded from all further evaluations. No significant differences were noted in the direction of testing for Young's modulus or the ultimate tensile stress (ANOVA, $p > 0.824$ and $p > 0.613$, respectively).

At 2 weeks, a decrease of approximately 40% in the median ultimate tensile strength was seen, while no changes in Young's modulus were seen compared with day 0 values. At 4 and 6 weeks, the corresponding decreases versus day 0 values were approximately 84% and 81% in the median ultimate tensile strength and 70% and 65% for Young's modulus, respectively. Statistical differences were confirmed in both the change in median ultimate tensile strength and Young's modulus over time (Kruskal–Wallis test, $p < 0.0001$ for both) and for the differences in ultimate tensile strength between week 2 and weeks 4 and 6 (Mann–Whitney test, $p < 0.0001$ for both) (Figure 5). Young's modulus was significantly different between all three time points (2 weeks and 4 weeks, 2 weeks and 6 weeks, 4 weeks and 6 weeks; $p < 0.0001$, $p < 0.0001$, and $p < 0.021$, respectively) (Figure 6). A significant increase in Young's modulus was noted between weeks 4 and 6.

Mechanical remodeling of fascia/peritoneum juxtaposed to incision and PADM

The ultimate tensile stress of fascia repaired with sutures only was significantly greater than that of fascia repaired with PADM at 6 weeks (Kruskal–Wallis, $p < 0.001$). The median ultimate tensile stress of fascia repaired with PADM was 1.82 MPa compared with 4.28 MPa for fascia repaired with sutures only (Figure 7). The sum of the average ultimate tensile stress of fascia from PADM repair and the ultimate tensile stress of the PADM itself was similar to the ultimate tensile stress of fascia from the suture-only group. Young's modulus of the fascia from the suture-only group trended greater than Young's modulus of the PADM repair group, although not quite statistically significant (Kruskal–Wallis, $p > 0.076$). The median Young's modulus of fascia repaired with PADM was 13.19 MPa compared with 20.51 MPa for fascia repaired with sutures only (Figure 7).

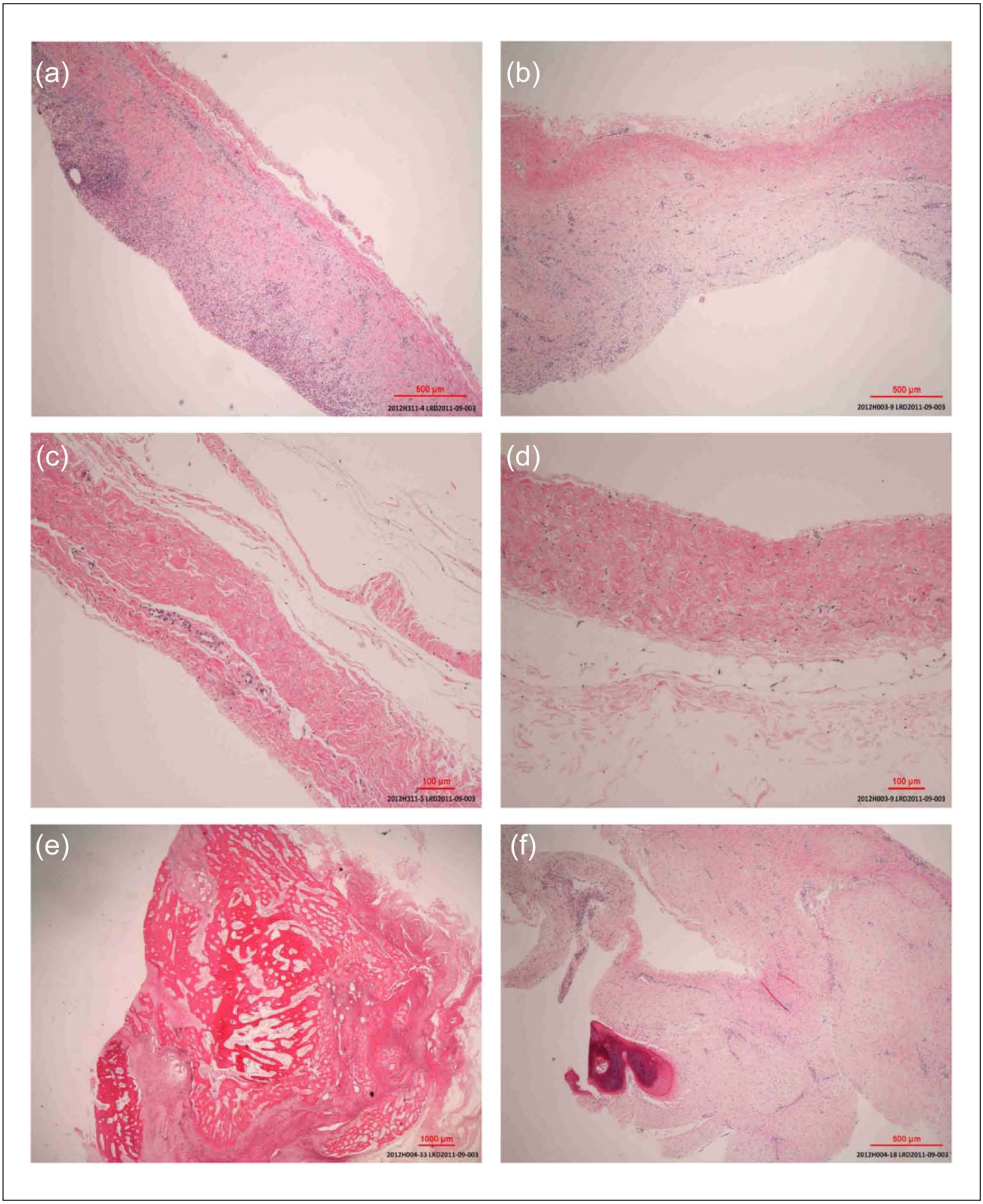

Figure 4. Hematoxylin and eosin staining of fascia tissue. Inflammation in peritoneum and fascia below the abdominal rectus was minimal for both suture-only and non-cross-linked intact porcine-derived acellular dermal matrix (PADM) groups: (a, b, e) Suture-only repair and (c, d, f) PADM reinforced. The deep red staining in (e) and (f) is indicative of calcification.

Table 1. Average scores for graft repopulation, revascularization, and inflammatory cell response.

Time (days)	Graft repopulation	Graft revascularization	Inflammatory cell response
14	1.73	1.17	1.43
28	2.30	1.97	1.60
42	2.67	2.30	1.17

All values are an average of at least three slides from six different animals at each time point. In general, repopulation and revascularization of the graft increased with increasing time while inflammation decreased over time.

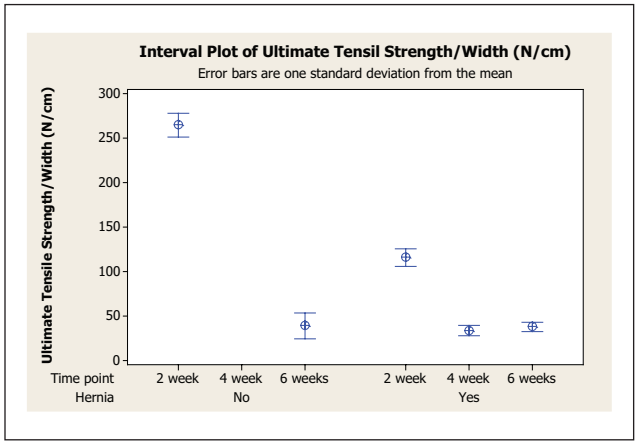

Figure 5. Retrospective evaluation of the ultimate tensile strength of herniated versus nonherniated animals demonstrated that non-cross-linked intact porcine-derived acellular dermal matrix (PADM) remodeling of herniated versus nonherniated animals and PADM number were significantly different (ANOVA, both $p < 0.0001$), as determined by a general linear model with hernia formation, PADM lot, and direction of testing as model factors. At the 4-week time point, all animals presented with a hernia post incision. The *x*-axis represents two groups: presence of hernia and time of euthanization following repair. The *y*-axis represents the ultimate tensile strength.

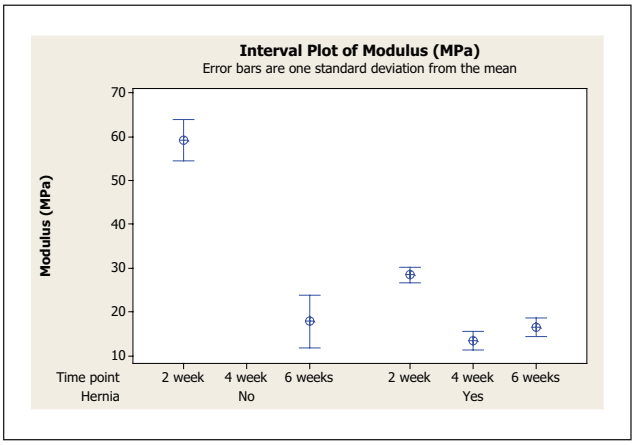

Figure 6. Within the herniated group, Young's modulus values were statistically different between all three time points (2 and 4 weeks, 2 and 6 weeks, 4 and 6 weeks; $p < 0.0001$, $p < 0.0001$, and $p < 0.021$, respectively). A statistically significant increase in Young's modulus was noted between weeks 4 and 6. The crossed circles represent the mean value of Young's modulus for each group. At 4 weeks, all animals presented with hernias following the 3 weeks of incision. The *x*-axis represents two groups: presence of hernia and time of euthanization following repair. The *y*-axis represents Young's modulus.

Mechanical testing of abdominal rectus muscle across the repair site

No statistical differences were noted in the ultimate tensile strength of muscle tested between both PADM and suture-only groups at 6 weeks post repair (median ultimate tensile stress, 54 N/cm for PADM versus 61 N/cm for suture-only groups; Kruskal–Wallis, $p > 0.629$) (Figure 8).

Microarray analysis

Only tissues from herniated animals were used in the microarray analysis; 404 probes were statistically differentially expressed at 6 weeks between the suture-only and PADM groups (*t*-test, $p < 0.05$). Hierarchical clustering was used to cluster gene profiles of the 404 differentially expressed genes. In hierarchical clustering, genes with similar expression patterns are grouped together and are connected by a series of branches, forming the clustering tree. Branches most closely connected have the most similar gene expression. Hierarchical clustering analysis demonstrated that the gene profile in time 0 animals (animals with no defects; biopsies harvested at time of incision creation) was more similar to PADM-reconstructed animals compared with the suture-only group. Among PADM-reconstructed animals, the week 6 time point showed the most similarity to the native state and the week 2 time point showed the most similarity to the herniated state (Figure 9). Table 2 contains the 10 most differentially expressed genes at 6 weeks in the study groups.

Discussion

Meshes for hernia repair need to be specifically designed for their applications. An ideal biological matrix for a reinforced closure needs to provide structural integrity at the time of implantation and a scaffold for regeneration as the body heals. Intact ECM scaffolds implanted in vivo will

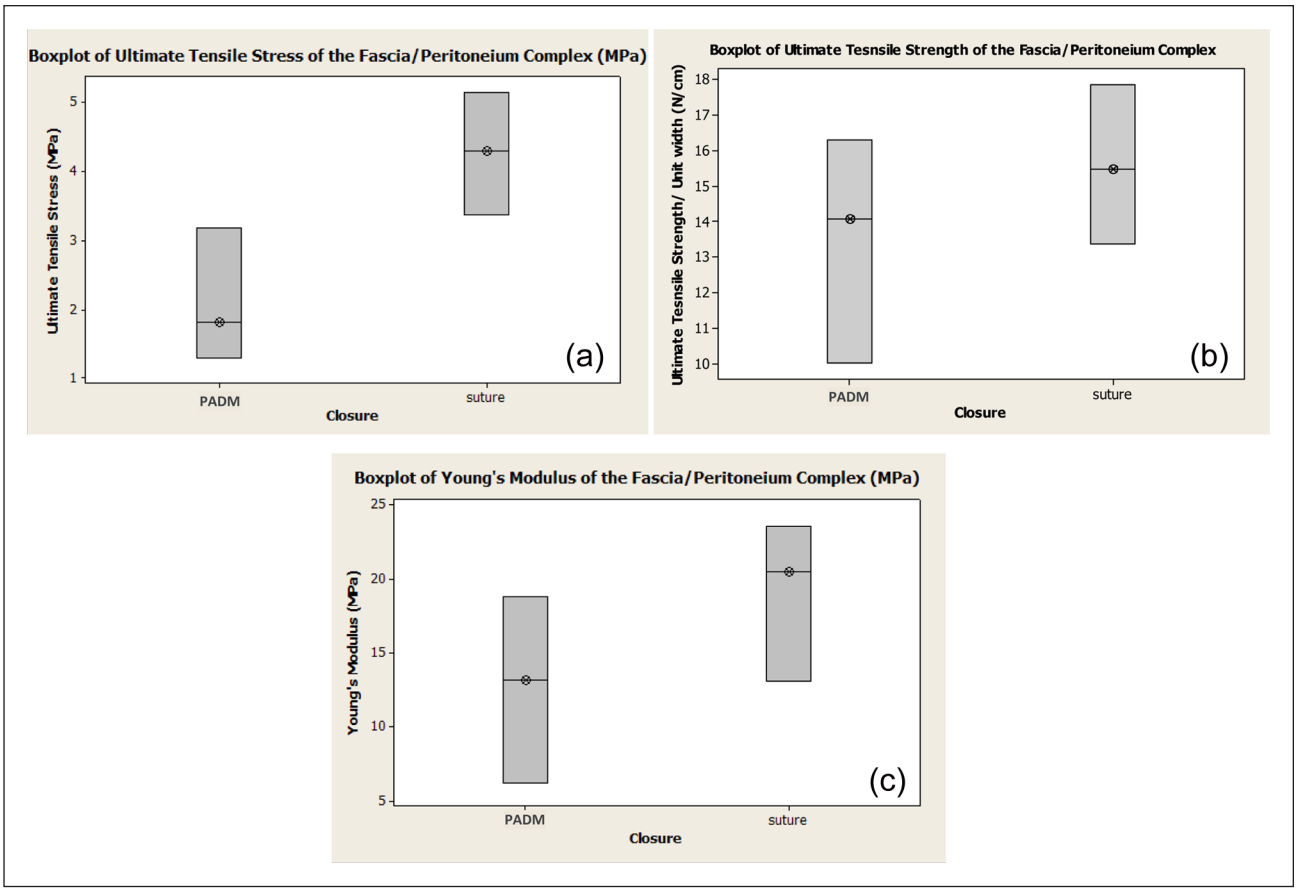

Figure 7. (a) Ultimate tensile stress, (b) ultimate tensile strength, and (c) Young's modulus of the peritoneum/fascia complex at 6 weeks post hernia repair. The crossed circles represent the mean value and the box represents 1 standard deviation from the mean. PADM: porcine-derived acellular dermal matrix.

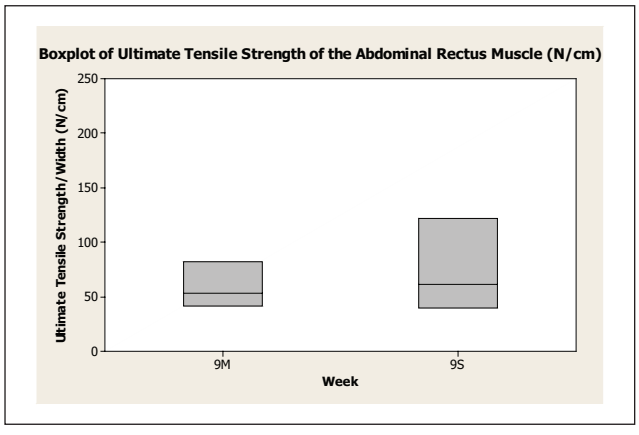

Figure 8. Ultimate tensile strength of the abdominal rectus muscle at 6 weeks post hernia repair.

remodel both mechanically as well as biologically over time. Returning the normal genetic profile at the injury site is essential for a return to normal functioning and wound healing. To date, an excess of 14 commercially available biologically derived matrices for hernia repair are currently in clinical use,[6,18] but there are relatively few short- and long-term preclinical outcome studies on biological matrices in the literature, with even fewer studies with clinically relevant settings and loading. Moreover, being derived from a natural tissue is not sufficient to elicit positive responses, as material processing has been shown to affect integration into the host.[19] This study was focused on understanding the biological and mechanical efficacy of a biologically derived intact ECM scaffold prepared using the Strattice-processing method in a clinically applicable porcine model of a large ventral hernia.

Large incisional hernias present a complex milieu of biological and mechanical signaling and remodeling that can influence the remodeling of biological materials used for repair. Three weeks after incision, a well-defined hernia ring along with substantial inflammation and swelling was noted in the abdominal rectus and skin flap in this study. Although this bodes well for secondary flap healing, inflammation in the abdominal rectus muscles and surrounding structures makes repairing the hernia more challenging. Additionally, inflammation is associated with high

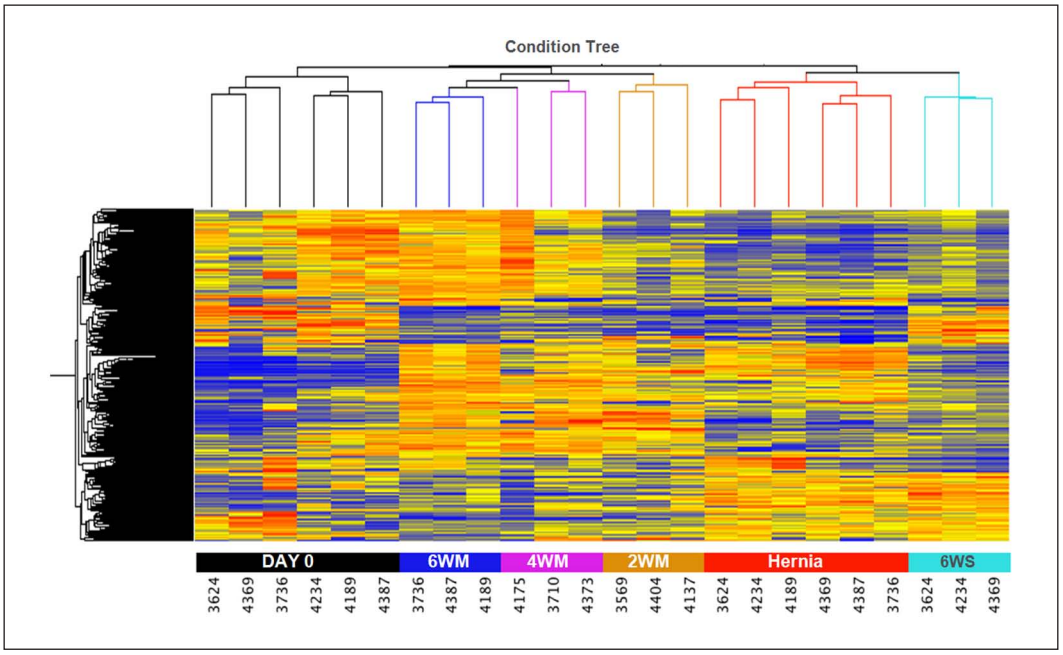

Figure 9. Differentially expressed genes at 2, 4, and 6 weeks in the suture-only versus non-cross-linked intact porcine-derived acellular dermal matrix (PADM) groups (>twofold, $p < 0.05$, 404 probes) normalized to mean expression across 24 samples compared with untreated control. Red/orange indicates high expression, yellow indicates medium expression, and blue indicates low expression. Gene expression profiles were clustered to group most similar groups together. The untreated control and 6-week PADM repair present the most similar gene expressions. A progression in the gene expression toward a normal untreated condition is noted in the PADM-repaired group (M) over 2, 4, and 6 weeks. In comparison, the 6-week suture-only groups (S) were least similar to the untreated control.

protease activity,[20,21] which is capable of degrading biological materials. ECM scaffolds implanted in such fields need to be able to support physiologically relevant loading and avoid recurrence, even in the presence of protease activity. In this study, inflammation and swelling were increasingly reduced as noted by gross observations in PADM-reinforced animals at 2, 4, and 6 weeks. Furthermore, between 4 and 6 weeks after repair, PADM remodeling was minimal. Thus, it appears there exists a window immediately following PADM placement that the PADM will undergo maximum remodeling prior to wound healing in this model.

At no time point was it noted that the absolute tensile strength of the PADM was below that of the surrounding fascia, which is important in terms of preventing hernia recurrence. Similar results in tensile strength were noted in previous primate studies.[9,19] The average minimum ultimate tensile stress of remodeled PADM occurred at 4 and 6 weeks. In comparison to the Förstemann abdominal wall model,[22,23] the average minimum ultimate tensile strength of the PADM was at least 25 times greater than the average loading experienced in a human abdominal wall.[22,23] Furthermore, the average Young's modulus of the PADM and fascia at 6 weeks was similar. Since Young's modulus is a measure of the stress needed to deform a material, and because the matrix and abdominal wall are in contact in a complete closure repair, both the matrix and the peritoneum/fascia complex will work in concert to resist strains and loads in the abdominal wall, adding to the ability of the repair to withstand bulging and hernia recurrence. This remodeling in mechanical properties is consistent with previous rat study data we generated[24] and is also generally noted when implanting collagen-based tissues in vivo.[25–27]

The histological evaluation of implanted PADM in this study demonstrated PADM remodeling into fascia-like tissue. On average, implanted PADM was moderately revascularized in 2 weeks and highly vascularized in 4 weeks. Repopulation of PADM followed similar trends. Minimal to no inflammation and scarring was observed in the PADM or peritoneum/fascia complex behind the PADM at any time point. However, significant scarring and heterotopic bone formation were observed with suture regions in the suture-only group. Hypertrophic bone formation is commonly associated with blunt trauma and subsequent deep-tissue bleeding. Symptoms include restricted range of motion and severe pain when muscles are used. Such results are not consistent with functional repair of a herniated abdominal wall.

The success rate of hernia formation in this model was approximately 71%. The size of incisions created to facilitate herniation was more than twice that in previous publications,[17,28] and incisions were created along the linea alba, a highly nonvascular tissue. This presents a greater

Table 2. Ten most differentially expressed genes at 6 weeks, suture-only versus PADM group*.

Systematic	Gene symbol	Ratio	*p*	Gene name	Description
A_72_P632350	*KRT8*	17.588	1.53E−02	Keratin 8	Sus scrofa keratin 8 (*KRT8*), mRNA [NM_001159615]
A_72_P343443	*SPOCK3*	12.980	3.81E−02	SPARC/osteonectin, cwcv, and kazal-like domains proteoglycan (testican) 3	PREDICTED: Sus scrofa SPARC [XM_001927757]
A_72_P473418	*LOC100154395*	12.174	2.76E−02	Protein NOV homolog	Uncharacterized protein [Source: UniProtKB/TrEMBL; Acc: F1S279] [ENSSSCT00000006586]
A_72_P517687	*MEST*	11.135	1.49E−02	Mesoderm-specific transcript homolog (mouse)	Sus scrofa mesoderm-specific transcript homolog (mouse) (*MEST*), mRNA [NM_001128471]
A_72_P743157	*CYP3A46*	6.923	4.11E−02	Cytochrome P450 3A46	Sus scrofa cytochrome P450 3A46 (*CYP3A46*), mRNA [NM_001134824]
A_72_P413508	*MMP1*	4.906	2.90E−02	Matrix metallopeptidase 1 (interstitial collagenase)	Sus scrofa matrix metallopeptidase 1 (interstitial collagenase) (*MMP1*), mRNA [NM_001166229]
A_72_P449126	*PAK7*	0.146	1.72E−02	p21 protein (Cdc42/Rac)-activated kinase 7	Uncharacterized protein [Source: UniProtKB/TrEMBL; Acc: F1SBK7] [ENSSSCT00000007732]
A_72_P415723	*LOC100169745*	0.139	4.77E−03	Cellular retinoic acid–binding protein 1	Sus scrofa clone Clu_88255. scr.msk.p1.Contig1, mRNA sequence [AY610183]
A_72_P407178	*LOC100037976*	0.107	3.85E−02	Soluble RANKL	Uncharacterized protein [Source: UniProtKB/TrEMBL; Acc: F1RJX1] [ENSSSCT00000010336]
A_72_P684857	*CYP11A1*	0.077	3.64E−02	Cytochrome P450, family 11, subfamily A, polypeptide 1	Sus scrofa mRNA, clone: OVRM10128H04, expressed in ovary [AK235955]

Red cells indicate a decrease in gene expression and blue cells indicate an increase in gene expression.
*More than twofold, $p < 0.05$, 404 probes.

challenge for wound healing. Given the unprecedented nature of this work, longer incisions were avoided in the interest of animal welfare. However, on completion of this study and realization of the robustness of the skin flaps created, future studies should incorporate longer incisions with fewer interrupted sutures to close the primary incision and elicit a higher herniation rate. Furthermore, this model may be enhanced by extending the time between incision creation and hernia repair. As noted earlier, there is still a large amount of inflammation and swelling present in the abdominal rectus and the skin flap 3 weeks after incision; additional time between incision and repair should allow for inflammation resolution as well as further maturation of the hernia rings and complete hernia sac development.

Although hernia recurrence rates were not evaluated, this work is a first step in creating a truly complex hernia animal model. The hierarchical clustering of microarray data demonstrates a return to a native (no hernia) gene expression state in the matrix-repaired animal over time. Two genes of notable interest are the *SPARC* gene, which regulates the glycoprotein osteonectin, a molecule implicated in several biological functions including the mineralization of bone and cartilage,[29,30] and *p21*, which functions as a regulator of cell cycle and regeneration.[31,32] Suture-only repairs presented a gene profile more similar to the herniated group. It must be noted that one animal in the suture-only group had suture failure at 6 weeks. Even though the abdominal wall of this animal did not herniate, notable weakness in the abdominal wall at the suture site was seen at the time of explant gross observations. On average, closure stiffness in the suture-only group was greater than that of the PADM-reinforced group (Kruskal–Wallis, $p > 0.076$). These results correlate well with the noted bone hypertrophy and overexpression of SPARC glycoprotein (secreted protein, acidic, rich in cysteines; also known as osteonectin) in the suture-only group and are in line with

results reported by DuBay et al.,[13] who found that matrix incisional herniorrhaphy resulted in a more elastic early postoperative abdominal wall compared with primary suture repairs in a rat model. DuBay et al. also demonstrated that a compliant abdominal wall after repair was more predictive of a lower hernia recurrence rate.

Conclusion

In this study, we evaluated a large-animal incisional hernia model and examined the biological and mechanical revitalization of a biologically derived matrix. The model is able to simulate the acute gross biology of an incisional hernia, with formation of the dense hernia ring and bowel protrusion from the abdominal cavity; however, this model still lacks the collagen gene deficiency[33] and comorbidities associated with clinical patients. The hernias formed were repaired using standard techniques of primary closure with and without PADM reinforcement, and outcomes from repairs were similar to clinical and literature-based expectations. Additionally, the mechanical integrity of the repair techniques was also in agreement with previous animal models of smaller scale. Suture-only repairs resulted in what appeared to be a scarring response, while biological matrix repairs provided a more elastic abdominal wall in the early postoperative period. These findings were corroborated with gene expression data. Taken together, the mechanical and biological data provide further evidence for the preference of biological matrix repair over suture-only closure for hernia repair.

Declaration of conflicting interests

Aubrey I. Delossantos, Neil L. Rodriguez, Paarun Patel, and Michael G. Franz are employees of LifeCell Corporation, Inc., Branchburg, NJ, USA. Gary A. Monteiro was an employee of LifeCell Corporation, Inc., at the time this study and article were completed. Christopher T. Wagner was an employee of LifeCell Corporation, Inc., at the time this study was developed and executed.

Funding

This work was funded by LifeCell Corporation, Inc., Branchburg, NJ, USA. Editorial support was provided by Peloton Advantage, LLC, Parsippany, NJ, USA and funded by LifeCell Corporation, Inc.

References

1. Luijendijk RW, Hop WC, van den Tol MP, et al. A comparison of suture repair with mesh repair for incisional hernia. *N Engl J Med* 2000; 343(6): 392–398.
2. Burger JW, Luijendijk RW, Hop WC, et al. Long-term follow-up of a randomized controlled trial of suture versus mesh repair of incisional hernia. *Ann Surg* 2004; 240(4): 578–583.
3. Vrijland WW, van den Tol MP, Luijendijk RW, et al. Randomized clinical trial of non-mesh versus mesh repair of primary inguinal hernia. *Br J Surg* 2002; 89(3): 293–297.
4. Boruch AV, Nieponice A, Qureshi IR, et al. Constructive remodeling of biologic scaffolds is dependent on early exposure to physiologic bladder filling in a canine partial cystectomy model. *J Surg Res* 2010; 161(2): 217–225.
5. Bellows CF, Alder A and Helton WS. Abdominal wall reconstruction using biological tissue grafts: present status and future opportunities. *Expert Rev Med Devices* 2006; 3(5): 657–675.
6. Smart NJ, Marshall M and Daniels IR. Biological meshes: a review of their use in abdominal wall hernia repairs. *Surgeon* 2012; 10(3): 159–171.
7. Cevasco M and Itani KM. Ventral hernia repair with synthetic, composite, and biologic mesh: characteristics, indications, and infection profile. *Surg Infect (Larchmt)* 2012; 13(14): 209–215.
8. Breuing K, Butler CE, Ferzoco S, et al. Incisional ventral hernias: review of the literature and recommendations regarding the grading and technique of repair. *Surgery* 2010; 148(3): 544–558.
9. Connor J, McQuillan D, Sandor M, et al. Retention of structural and biochemical integrity in a biological mesh supports tissue remodeling in a primate abdominal wall model. *Regen Med* 2009; 4(2): 185–195.
10. De Castro Bras LE, Shurey S and Sibbons PD. Evaluation of crosslinked and non-crosslinked biologic prostheses for abdominal hernia repair. *Hernia* 2012; 16(1): 77–89.
11. Hodde J. Extracellular matrix as a bioactive material for soft tissue reconstruction. *ANZ J Surg* 2006; 76(12): 1096–1100.
12. DuBay DA, Choi W, Urbanchek MG, et al. Incisional herniation induces decreased abdominal wall compliance via oblique muscle atrophy and fibrosis. *Ann Surg* 2007; 245(1): 140–146.
13. DuBay DA, Wang X, Adamson B, et al. Mesh incisional herniorrhaphy increases abdominal wall elastic properties: a mechanism for decreased hernia recurrences in comparison with suture repair. *Surgery* 2006; 140(1): 14–24.
14. DuBay DA, Wang X, Adamson B, et al. Progressive fascial wound failure impairs subsequent abdominal wall repairs: a new animal model of incisional hernia formation. *Surgery* 2005; 137(4): 463–471.
15. Bringman S, Conze J, Cuccurullo D, et al. Hernia repair: the search for ideal meshes. *Hernia* 2010; 14(1): 81–87.
16. Penttinen R and Gronroos JM. Mesh repair of common abdominal hernias: a review on experimental and clinical studies. *Hernia* 2008; 12(4): 337–344.
17. Melman L, Jenkins ED, Hamilton NA, et al. Early biocompatibility of crosslinked and non-crosslinked biologic meshes in a porcine model of ventral hernia repair. *Hernia* 2011; 15(2): 157–164.
18. Meintjes J, Yan S, Zhou L, et al. Synthetic, biological and composite scaffolds for abdominal wall reconstruction. *Expert Rev Med Devices* 2011; 8(2): 275–288.
19. Sandor M, Xu H, Connor J, et al. Host response to implanted porcine-derived biologic materials in a primate model of abdominal wall repair. *Tissue Eng Part A* 2008; 14(12): 2021–2031.
20. Parks WC, Wilson CL and Lopez-Boado YS. Matrix metalloproteinases as modulators of inflammation and innate immunity. *Nat Rev Immunol* 2004; 4(8): 617–629.

21. Page-McCaw A, Ewald AJ and Werb Z. Matrix metalloproteinases and the regulation of tissue remodelling. *Nat Rev Mol Cell Biol* 2007; 8(3): 221–233.
22. Förstemann T, Trzewik J, Holste J, et al. Forces and deformations of the abdominal wall—a mechanical and geometrical approach to the linea alba. *J Biomech* 2011; 44(4): 600–606.
23. Konerding MA, Bohn M, Wolloscheck T, et al. Maximum forces acting on the abdominal wall: experimental validation of a theoretical modeling in a human cadaver study. *Med Eng Phys* 2011; 33(6): 789–792.
24. Monteiro GA, Rodriguez NL, Delossantos AI, et al. Short-term in vivo biological and mechanical remodeling of porcine acellular dermal matrices. *J Tissue Eng* 2013; 4: 2041731413490182.
25. Bagnaninchi PO, Yang Y, El Haj AJ, et al. Tissue engineering for tendon repair. *Br J Sports Med* 2007; 41(8): e10.
26. Tischer T, Aryee S, Wexel G, et al. Tissue engineering of the anterior cruciate ligament-sodium dodecyl sulfate-acellularized and revitalized tendons are inferior to native tendons. *Tissue Eng Part A* 2010; 16(3): 1031–1040.
27. Sandmann GH and Tischer T. Tissue engineering of the anterior cruciate ligament and meniscus using acellularized scaffolds. In: Eberli D (ed.) *Tissue engineering*. Rijeka: InTech Open, 2010, pp. 437–458.
28. Deeken CR, Melman L, Jenkins ED, et al. Histologic and biomechanical evaluation of crosslinked and non-crosslinked biologic meshes in a porcine model of ventral incisional hernia repair. *J Am Coll Surg* 2011; 212(5): 880–888.
29. Stenner DD, Tracy RP, Riggs BL, et al. Human platelets contain and secrete osteonectin, a major protein of mineralized bone. *Proc Natl Acad Sci U S A* 1986; 83(18): 6892–6896.
30. Young MF, Kerr JM, Ibaraki K, et al. Structure, expression, and regulation of the major noncollagenous matrix proteins of bone. *Clin Orthop Relat Res* 1992; 281: 275–294.
31. Bedelbaeva K, Snyder A, Gourevitch D, et al. Lack of p21 expression links cell cycle control and appendage regeneration in mice. *Proc Natl Acad Sci U S A* 2010; 107(13): 5845–5850.
32. Rodriguez R and Meuth M. Chk1 and p21 cooperate to prevent apoptosis during DNA replication fork stress. *Mol Biol Cell* 2006; 17(1): 402–412.
33. Calaluce R, Davis JW, Bachman SL, et al. Incisional hernia recurrence through genomic profiling: a pilot study. *Hernia* 2013; 17(2): 193–202.